J Appl Electrochem (2013) 43:31–41
DOI 10.1007/s10800-012-0500-7

ORIGINAL PAPER

Impedance spectroscopic determination of effect of temperature on the transport resistances of an electro-electrodialysis cell used for concentration of hydriodic acid

Pradeep Kumar Sow · D. Parvatalu · Anil Bhardwaj · B. N. Prabhu · A. N. Bhaskarwar · Anupam Shukla

Received: 7 August 2012 / Accepted: 29 October 2012 / Published online: 8 November 2012
© Springer Science+Business Media Dordrecht 2012

Abstract Effect of temperature on different transport resistances of an electro-electrodialysis (EED) cell used for concentration of hydriodic acid (HI) was found by equivalent circuit modeling of the measured impedance response of the cell. The EED cell consisted of two compartments separated by Nafion 117 membrane and each compartment had a platinum electrode. Both the compartments were filled with aqueous solution of 55 wt% HI containing 0.5 M iodine. Impedance measurements were carried out at four different temperatures in the range of 308–353 K. Equivalent circuit for the cell consisted of a resistor for ohmic resistance of the cell, a Warburg element for the resistance due to diffusion boundary layer and a constant phase element for the resistance to transport of ions due to non-electro neutral heterogeneous transport layer at the membrane. Effect of temperature on impedance due to heterogeneous transport was lower than the Warburg impedance and the solution and membrane resistance. Effective capacitance of the heterogeneous transport layer was found to reduce with temperature. The dynamics of the heterogeneous transport layer along with the diffusional boundary layer were found to reduce with increase in the cell operating temperature.

Keywords Electro-electrodialysis · HI_x · Impedance spectroscopy · Iodine–sulfur cycle · Ion exchange membrane

P. K. Sow · A. N. Bhaskarwar · A. Shukla (✉)
Department of Chemical Engineering, Indian Institute of Technology, Hauz Khas 110016, New Delhi, India
e-mail: anupam@chemical.iitd.ac.in

D. Parvatalu · A. Bhardwaj · B. N. Prabhu
ONGC Energy Centre, IEOT, Panvel 410221, India

1 Introduction

Hydrogen is being considered as one of the most promising clean sources of energy for the future [1–3]. Various methods have been suggested for the hydrogen production, which can be chemical, thermal, electrochemical, or biological [4, 5]. However, among all the hydrogen production processes, thermochemical cycles have been suggested to be a viable option for large scale production of hydrogen [6, 7]. Thermo-chemical cycles, first proposed in 1970s, have high thermal efficiency as compared to other processes being explored for producing hydrogen from water and they also do not produce or release any green-house gases [7]. Iodine–sulfur (IS) cycle, developed by General Atomics, is the most promising of the thermo-chemical cycles with a theoretical efficiency of around 50 % [8]. The IS process mainly comprises three major reactions viz. the Bunsen reaction, decomposition of sulfuric acid (H_2SO_4) and hydriodic acid (HI) decomposition [8–10].

$$\text{Bunsen reaction: } I_2(l) + SO_2(g) + 2H_2O\ (l) \xrightarrow{393\,K} 2HI(aq) + H_2SO_4(aq) \quad (1)$$

$$\text{Sulfuric acid decomposition: } H_2SO_4(aq) \xrightarrow{1123\,K} H_2O(l) + SO_2(g) + (1/2)O_2 \quad (2)$$

$$\text{Hydrogen iodide decomposition: } 2HI(aq) \xrightarrow{723\,K} H_2 + I_2(l) \quad (3)$$

In the above mentioned three reaction-based scheme for the hydrogen production, iodine, sulfur and water act as recycling agents to facilitate decomposition of water into hydrogen and oxygen at lower temperature. In the traditional IS cycle, the Bunsen reaction was carried out by direct contact of sulfur dioxide with aqueous solution of iodine,

where excess amounts of water and iodine were used for higher conversion and separation of the two acid phases, respectively [10, 11]. Large amount of iodine also caused handling problems especially in HI decomposition section. An excess amount of iodine leads to formation of pseudo azeotropic HI_x solution (molar ratio of HI: $H_2O = 1{:}5$) making normal distillation difficult for further concentration of HI. Large amount of thermal energy is thus required to break the azeotrope and this adversely affects the thermal efficiency of the process [11–13]. One of the important aspects in the development of the IS cycle is reduction of the energy consumed so as to boost the overall thermal efficiency of the cycle, while the sulfur section (sulfuric acid decomposition) has been well established with little scope for further improvisation in terms of thermal efficiency. However, the iodine section still holds a substantial scope for reduction in the net energy consumed in the process [14] as HI_x concentration scheme is not well established, uses large fraction of total energy demand and therefore offers scope of substantial reduction in energy required. One of the recent developments toward this objective is use of ion-exchange membrane-based electro-electrodialysis (EED) process for concentration of HI_x solution [15–20].

Essentially an EED cell assembly consists of two compartments, both containing HI_x solution, separated by an ion exchange membrane (IEM) as shown in Fig. 1. For this system, cation exchange membranes are preferred over anion exchange membranes due to higher mobility of the protons in comparison to the anions (iodide ions) [15]. The following iodine–iodide redox reaction takes place at the electrodes in the electrochemical cell [16, 17]:

$$I_2 + 2e^- \leftrightarrow 2I^- \tag{4}$$

Cation exchange membrane allows selective permeation of protons from the anode to the cathode compartment. The protons transported to cathode compartment along with the iodide ions produced at the cathode leads to an increase in the concentration of HI in the catholyte and depletion of HI concentration in the anolyte. Studies on high temperature-based operation of EED cell has revealed that the overall cell resistance reduces with increase in temperature and hence affecting the electrical energy consumed for achieving same amount of HI concentration [16–20]. A common pattern observed in all the studies on the effect of temperature on the EED energy determining variables (H^+ transport number, and current efficiency) is that the transport number of proton though the IEM and the current efficiency of the process decrease with increase in temperature. While both of these adversely affect energy demand of EED cell, a proper explanation of this effect is lacking in the literature. Moreover, while the reduction in the overall resistance of the EED cell has been reported in the literature, the relative

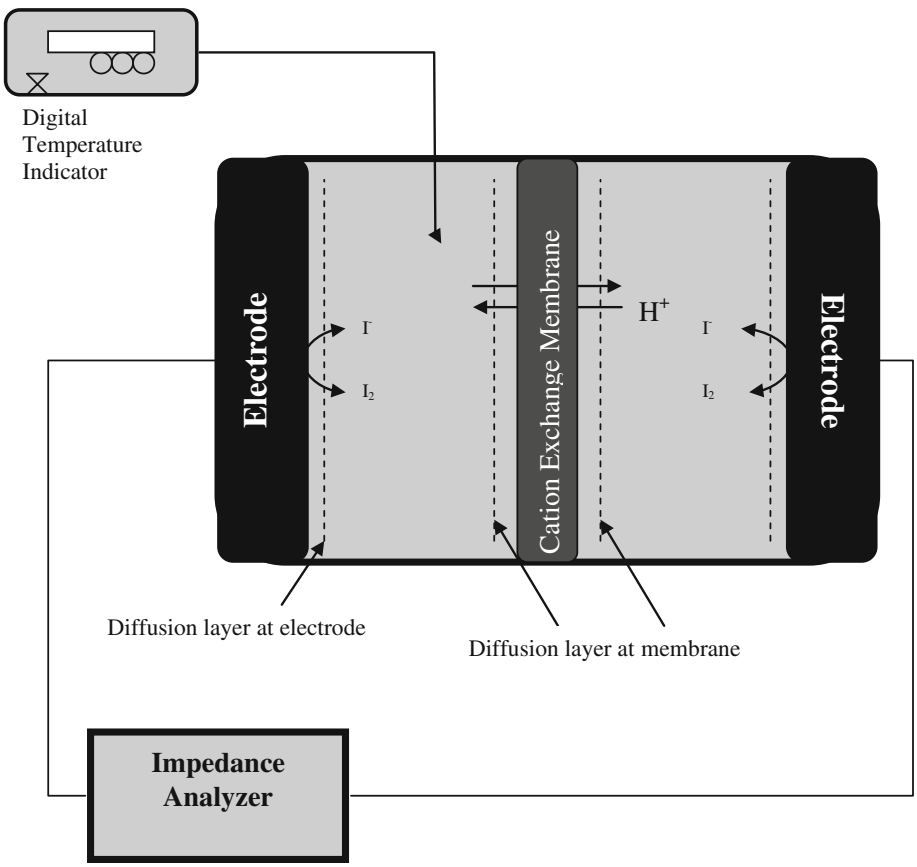

Fig. 1 Schematic diagram of the two-compartment electro-electrodialytic cell for concentration of hydriodic acid showing the electrolyte chambers housing the electrodes separated by a cation exchange membrane

magnitude of different resistance (impedance) components as a function of temperature is not reported. This work is an attempt to bridge this gap in the existing literatures using electrochemical impedance spectroscopy (EIS) as a tool for the system analysis.

Electrochemical impedance spectroscopy has been used as one of the ways to characterize the transport resistances of an electrochemical cell and ion-exchange membrane [21–31]. One of the most common methods used to understand the impedance response of the IEM is use of theoretical interpretations derived from the Nernst–Plank and Poisson equation model of the ionic transport process through the membrane systems [27–30]. Another way which has been widely used in the literature to explain the EIS data is through the use of equivalent circuit modeling [21, 22, 25, 26]. Electrochemical impedance spectroscopy data are interpreted in terms of various circuit elements (like resistance, capacitors, etc.) which represent the different transport resistances occurring inside an electrochemical cell. Electrochemical impedance spectroscopy technique can be used to separate out process that occurs simultaneously in time domain on the basis of relative dominance at various frequency ranges.

In the present work, single platinum electrode for redox reaction of I_2/I^- was analyzed using impedance spectroscopy. Impedance measurements were conducted on the platinum electrode of different area to determine the impedance due to different transport phenomena near electrode. Impedance measurements were taken at different temperatures on a two-compartment EED cell used for concentration of HI_x solution. The cell consisted of an anode and a cathode compartment separated by Nafion 117 membrane. Platinum electrodes were used in both the compartment. Identical aqueous solutions of 55 wt% HI with 0.5 M iodine were used as anolyte and catholyte in all the experiments. Electrochemical impedance spectroscopy spectra were taken at five different temperatures in the range of 308–353 K. The EIS spectra were validated using Kramers–Kronig transform before further analysis. An equivalent circuit model of the cell was developed for interpreting the measured impedance data at different temperatures and identifying the contributing transport resistance variation. The data obtained from the equivalent circuit modeling were then used further to evaluate the equivalent capacitance of the heterogeneous transport layer along with the dynamics (based on time constant) of the membrane process involved in the present system.

2 Experimental

All single electrode studies were conducted in a conventional three electrode setup with Ag/AgCl reference electrode. Platinum wire of diameter 0.5 mm was used as counter electrode, and studies were done in HI_x solution. Electrolyte solutions were prepared using 55 wt% hydriodic acid supplied by Merck Specialties Pvt. Ltd., and iodine supplied by Fischer Chemicals Ltd., without any further purification.

Single platinum electrode impedance spectroscopic experiments were conducted with varying electrode area from 0.0019 to 0.310 cm^2. The HI_x electrolyte solution was 55 wt% HI with 0.5 M iodine. The frequency (ν) of the perturbed AC signal was varied from 10 kHz to 3 Hz for the impedance studies.

Studies on the EED cell was conducted at different temperatures. Impedance measurements were performed on an unstirred two-compartment electrochemical cell made up of Teflon with a compartment volume of 12 ml each and having platinum electrodes with geometrical area of 0.310 cm^2. Nafion 117 membrane supplied by Electrochem Inc (USA) was placed between the two compartments with an exposed area of about 5 cm^2. Aqueous solution containing 55 wt% HI and 0.5 M iodine was used as catholyte and anolyte in all the experiments. Temperature of the EED cell system was varied by immersing the cell assembly in a water bath. Electrolyte temperature in the cell was continuously monitored using digital temperature indicators. The temperature was stabilized for 30 min before the start of the experiment. Impedance measurements were taken at four different temperature values of 308, 323, 333, 343, and 353 K. All the impedance measurements were done with a perturbed sinusoidal ac voltage signal of amplitude 5 mV in the frequency (ν) range of 4 kHz to 3 mHz using a potentiostat/galvanostat/ZRA (Gamry Instruments Inc, Model—Reference 600™). The applied AC voltage was kept in lower range (5 mV), also the DC bias voltage was kept to zero so as to maintain symmetry in the EED cell to minimize the non-linear distortion effects [28, 29]. The impedance data obtained as Nyquist, and bode plots was used for further analysis.

3 Results and discussion

3.1 Single electrode studies

Impedance response of platinum electrode of different exposed geometric area in HI_x solution was measured in the frequency range of 10 kHz to 3 Hz. Fifty five weight percentage aqueous HI solution containing iodine of concentration 0.5 M was used as electrolyte. Impedance responses of the electrode are shown in Figs. 2 and 3 in the form of Nyquist plots and bode plot, respectively. From the bode plot phase angle response (Fig. 3b), it can be observed that for the area of 0.0019 cm^2, two phase humps are observed

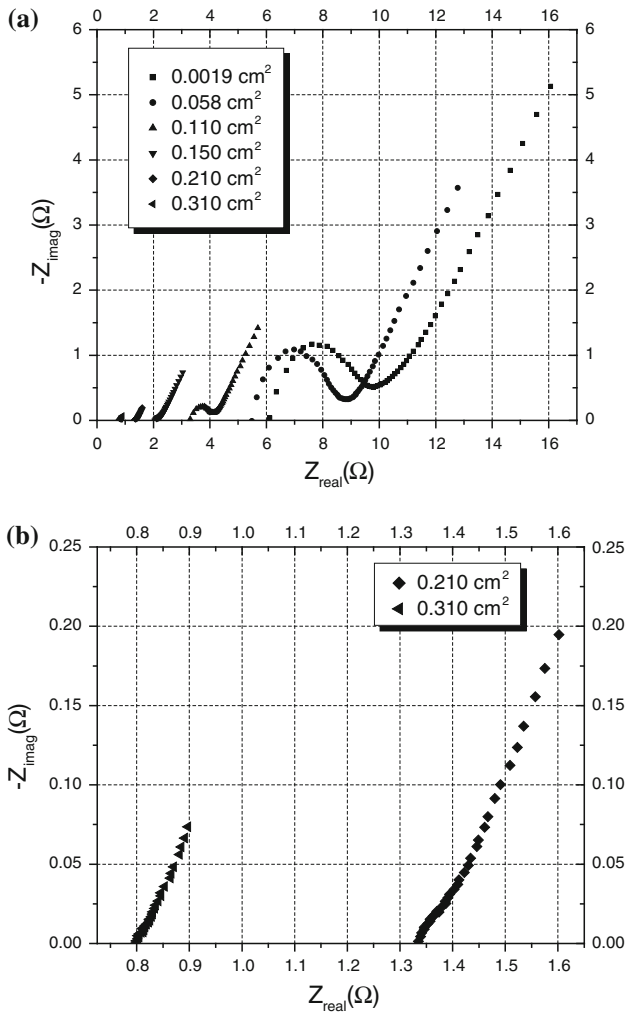

Fig. 2 Nyquist plot representation of single platinum electrode with variation of electrode area from 0.0019 to 0.310 cm^2. **a** Nyquist plot for variation of area from 0.0019 to 0.310 cm^2. **b** Magnified view of the nyquist plot for area 0.210 and 0.310 cm^2

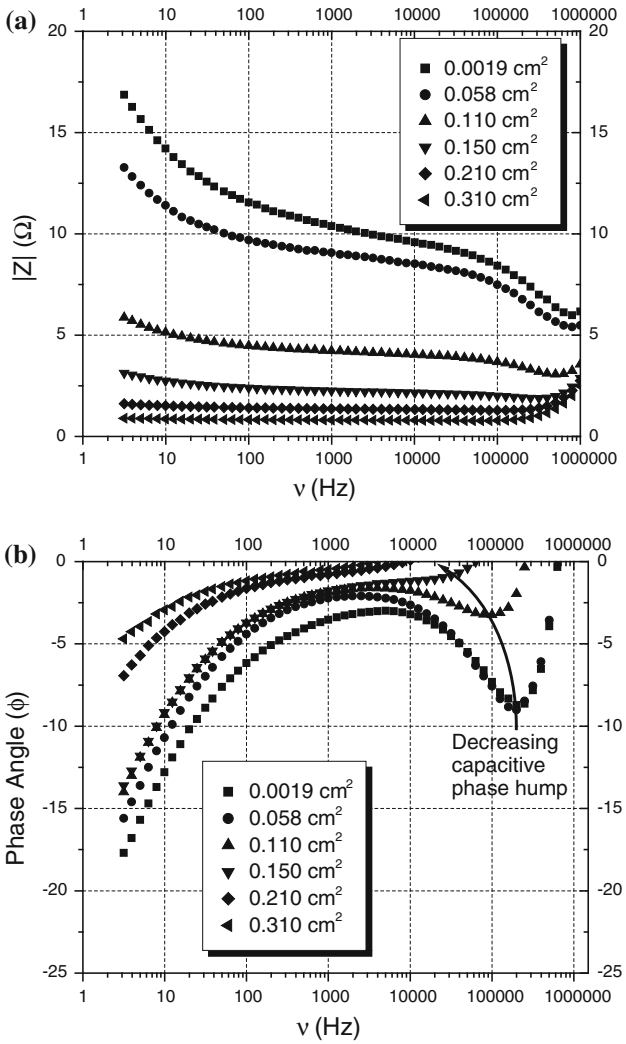

Fig. 3 Bode plot representation of single platinum electrode with variation of electrode area from 0.0019 to 0.310 cm^2. **a** Variation of total impedance |Z|. **b** Variation of phase angle with frequency as a function of electrode area varying from 0.0019 to 0.310 cm^2

each corresponding to the two capacitive loops observed in the Nyquist plots. The phase angle response in the bode plot suggests that the phase hump corresponding to the first capacitive loop reduces with increasing the electrode area from 0.0019 to 0.310 cm^2. Real axis intercept for the Nyquist plot corresponding to the electrode area of 0.0019 cm^2 was observed at a frequency of 631 kHz while for the electrode area of 0.310 cm^2, the Nyquist intercept was observed at 3,000 Hz. Prominent capacitive loop was observed for exposed electrode area of 0.0019 cm^2 (Fig. 2a). Diameter of the capacitive loop diameter decreased with increase in the electrode area and nearly disappears for electrode area of 0.310 cm^2 leaving only a straight line in the experimental frequency region (Fig. 2b). The residual straight line corresponded to impedance response at low frequencies and represents the impedance associated with resistance to transport of reactant to the electrode (mass transfer effect) [32, 33]. Thus, mass transfer resistance became dominant as the electrode area was increased and charge transfer resistance became negligible as the electrode area was increased beyond 0.310 cm^2. Similar results of negligible contribution of electrode charge transfer resistance have been reported in the literature for the impedance response of HI_x system [18, 26]. Yoshida et al. [20] also reported that the total electrode overpotential was negligibly low compared to the total potential drop across the cell which are consistent with our findings.

3.2 Studies on EED cell

3.2.1 Kramers–Kronig (K–K) analysis

Consistency of impedance data was examined by fitting it to Kramer–Kronig (K–K) relation using method suggested

by Boukamp [34] used in Gamry Echem analyst™. The K–K fit is obtained by fitting a generalized model to the impedance spectra obtained for the electrochemical system under consideration [35]. Figure 4a shows the K–K fitted data at 308 K. The K–K fit was found to be good and the residual error plot has been shown in Fig. 4b. It can be seen that the fit is extremely close at higher frequency ($\Delta Z/Z < 0.0005$); however, the relative residual error ($\Delta Z/Z$) increases slightly (~ 0.002) for both the real as well as imaginary component, as the frequency is further lower beyond ~ 5 Hz. However, the maximum residual error was found to be negligible (<0.0025). Kramer–Kronig fitting was done for the data obtained at all the temperature ranging from 308 to 353 K. The K–K fit for all the temperature showed similar trends. The overall reported goodness of fit was found from the analyst software and were found of order $\sim 10^{-5}$–10^{-7} for all the temperature ranges. The residual error values and the goodness of fit data prove the data to be linear, causal, and stable.

3.2.2 General trend

Impedance response of the cell at all the temperatures showed similar qualitative behavior, and Fig. 5 shows the response of the cell at 308 K in the form of both the Nyquist and the Bode plots. Figure 5a (Bode plot) shows that magnitude of impedance (|Z|) was nearly constant in high frequency range (10^3 –100 Hz) with nearly zero-phase angle (ϕ) indicating that this was the combined ohmic response of the membrane and electrolyte of the cell [21, 25, 32, 33, 36]. Figure 5b (Nyquist plot) shows the impedance response of the cell in form of a capacitive loop with intercept on real axis at high frequency corresponding to the ohmic response of the cell. Imaginary part of impedance was negligible at high frequencies (10 kHz–50 Hz). Also, the variation in real part of impedance was negligible at high frequencies. Both the capacitive loop and its intercept with real axis decreased with temperature (Fig. 6a). The lowering of the diameter of capacitive loop

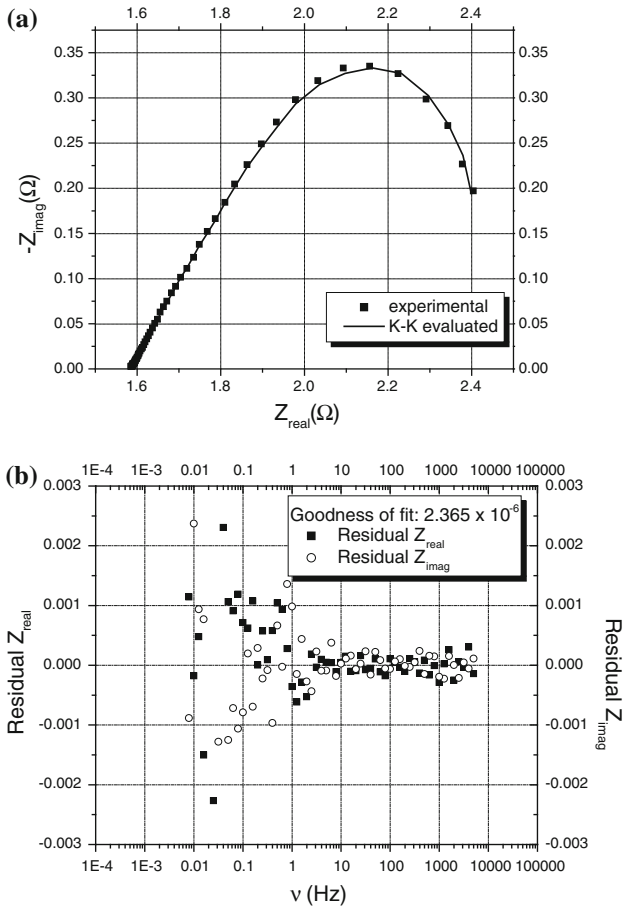

Fig. 4 Kramers–Kronig analysis of the impedance spectra at 308 K **a** Nyquist plot with K–K fit, **b** variation of residual real and imaginary impedance with frequency

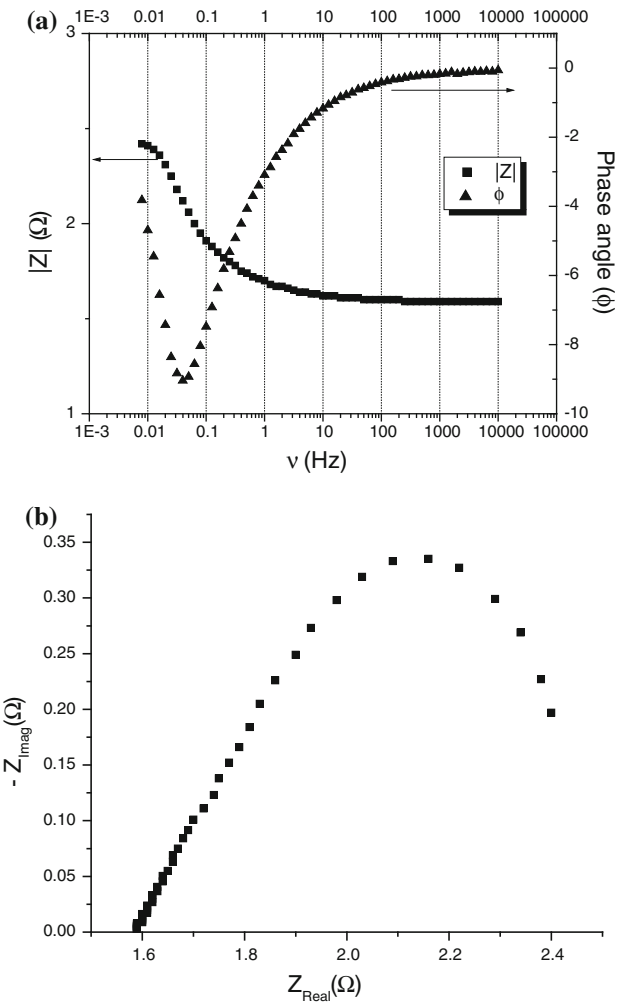

Fig. 5 Impedance response of the EED cell at 308 K represented by the **a** Bode plot, **b** Nyquist Plot

with reduction in temperature (Fig. 6a) can be inferred as the decrease in the complex impedance while the corresponding decrease in real axis intercept value indicated decrease in ohmic resistance. A distorted semi-circular shape of Nyquist plot indicated the presence of more than one process with different time constants. Further analysis was conducted using equivalent circuit modeling.

In the present system, the analysis is dependent on the symmetric response of the EED cell system across the membrane. The equilibrium potential of the cell was used as a parameter for the symmetric response of the system which was evaluated for each temperature and was found to be close to zero (<300 μV). The near zero value of the equilibrium potential is indicative of symmetric system.

3.2.3 *Equivalent circuit model for the cell*

A simple way to interpret impedance response of an electrochemical cell is to develop a circuit (called equivalent circuit) having same impedance response as that of the cell. The various elements of the circuit can be related to the different physical process occurring in the cell that offers resistance to the transport of current carrying species [21, 22, 32, 33].

The conventional EED cell comprises two electrodes at which the iodine–iodide redox reaction occurs. The electrode dynamics schematic diagram is shown in Fig. 7. The reacting species at the electrode surface can form an electrical double layer (EDL) at the surface which behaves as a capacitor-type circuit element. However, two different double layers are supposed to form at the anode and cathode, respectively. In the present impedance spectra, no two distinct capacitive semicircles are observed. This suggested that the time constant of the two EDLs are nearly equal. In addition to EDL, a diffusion boundary layer (DBL) exists near an electrode and transport of electroactive species from bulk to the electrode surface is through the DBL. The impedance response of a DBL can be simulated with a Warburg impedance. Conventionally, the Warburg impedance can be defined as the frequency dependent impedance (dependence of $\omega^{-0.5}$) due to diffusive resistance to the transport of the electroactive species. Though different kind of Warburg impedances have been defined in the literature broadly as infinite Warburg, bounded Warburg, and porous bounded Warburg, defined depending on the physical conditions prevailing during the transport process [32, 33, 35]. The most general form of Warburg impedance is infinite Warburg which refers to an infinite medium. Mathematically, it is expressed as [33]:

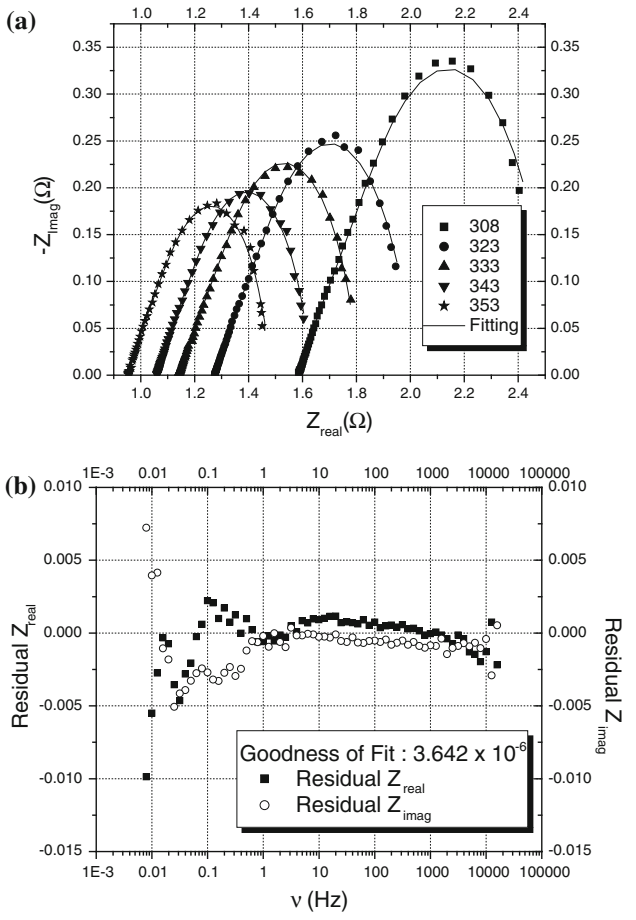

Fig. 6 **a** Nyquist plot representation of the impedance responses of the EED cell at five different temperatures in the range of 308–353 K along with model fit using equivalent circuit model. **b** Residual error ($\Delta Z/Z$) obtained for the equivalent circuit model fitting for temperature 308 K

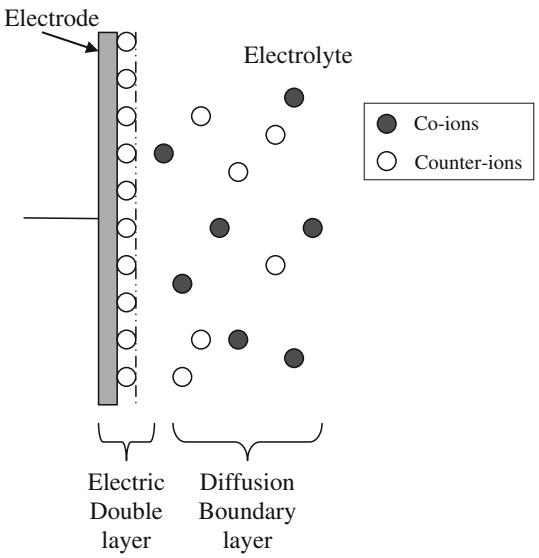

Fig. 7 Figure shows the electrode dynamics and the electrode phenomenon. The *dashed line* shows the outer helmholtz plane (*OHP*) for the EDL

$$Z_w = \frac{RT}{nFA\sqrt{j\omega}}\left[\frac{1}{c_R\sqrt{D_R}} + \frac{1}{c_O\sqrt{D_O}}\right] \quad (5)$$

Conventionally, the electrode response for a single electrochemical reaction coupled with mass transfer is modeled by a Randles circuit shown in Fig. 8a [32, 33]. However, in the discussion about the single electrode, it was found that the electrode charge transfer resistance is negligible and the response is dominated by the mass transfer resistance. In order to model diffusional impedance for the DBL, Warburg element (simulated using CPE) has been employed. The equivalent circuit for the response of DBL and consists of a Warburg circuit element in parallel to a leak ohmic resistance for the DBL (Fig. 8b).

Transport of H^+ ions near ion-exchange membrane (IEM) consists of two different processes in series along with ohmic resistance of the membrane. Figure 8c shows the equivalent circuit for the IEM system in HI_x electrolyte solution. Similar equivalent circuits have been reported in the literature for explaining the electrical response of the IEM systems [21, 22, 25, 26]. First part corresponds to the ohmic resistance of the IEM. The second component consisting of a parallel combination of a capacitive element and an ohmic (leak) resistance simulates the electrical double layer formed at the membrane surface (pores). This double layer is termed as the heterogeneous transport (HT) layer. The third part simulates the response of DBL near membrane and consists of a Warburg element in parallel to an ohmic (leak) resistance.

Overall response of the EED cell can be simulated by connecting the equivalent circuits for the two electrodes and membrane in series. In order to simplify the equivalent circuit of the EED cell, similar circuit elements can be combined (i.e., all the capacitive elements can be combined and all the Warburg elements can be combined). The resultant equivalent circuit of the EED cell is shown in Fig. 8d, consisted of three parts. The first part was a resistor (R_{sm}) to account for the ohmic resistance of the solution and the membrane. Each of the other two parts consisted of a parallel combination of a capacitance and a Warburg element with a resistor. In light of the results of single electrode system, where the charge transfer resistance became negligible at electrode area higher than 0.310, it can be concluded that the total capacitive response of the EED cell was primarily due to the HT layer of the IEM.

In general, use of ideal capacitor element does not give good match with the experimental data as the capacitive elements in real system are spatially distributed and also the overall effect is result of a number of relaxation processes of different time constants [21, 32, 33]. A constant phase

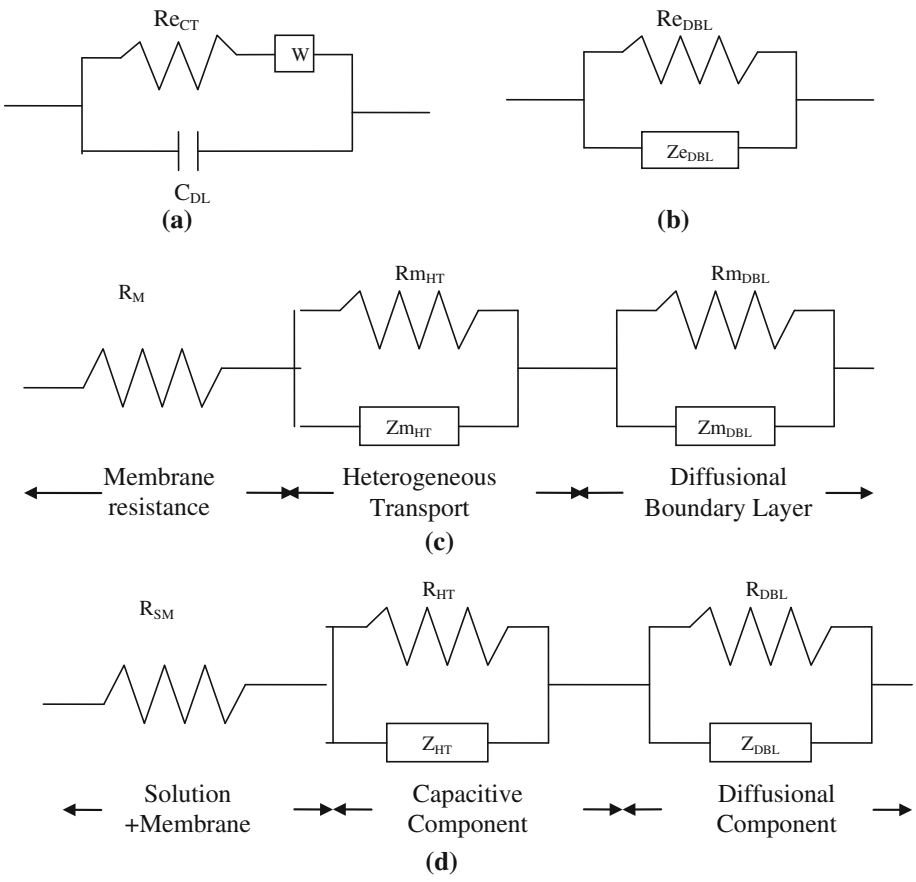

Fig. 8 Equivalent circuit representation of various components of EED cell **a** randles circuit for electrode reaction with mass transfer effect, **b** electrode reaction without EDL, **c** equivalent circuit for the IEM system, **d** combined equivalent circuit for EED cell system

element (CPE) gives better match with experimental data and is generally used in equivalent circuits. A CPE can represent all types of impedance behavior and is expressed as

$$-Z_{\text{imag}} = \frac{1}{Y_0}(j\omega)^{-n} \tag{6}$$

where Y_0 is the admittance (S.s^{n}) and n is the empirical parameter with value between 0 and 1. This value of n determines the nature of CPE. When n is close to a value of 0.5, the CPE is called Warburg impedance and is due to the resistance of DBL to the transport of ions. Values of n close to 1 and -1 indicate that the CPE represents capacitance-like and inductance-like behavior, respectively. A HT layer gives impedance response similar to that of a CPE with n value close to -1. Mathematically, it can be seen from the Eq. (6) that with value of $n = 0.5$, the CPE equation represents Eq. (5) with

$$Y_0 = \frac{RT}{nFA}\left[\frac{1}{c_{\text{R}}\sqrt{D_{\text{R}}}} + \frac{1}{c_{\text{O}}\sqrt{D_{\text{O}}}}\right]$$

It has also been reported in the literature that the Warburg impedance can be modeled using a CPE with the value of $n \sim 0.5$ [21, 26]. Moreover, as the electrochemical system does not behave ideally, the use of CPE (with $n \sim 0.5$) instead of Warburg is justified.

Of all the parameters values required for simulation of the impedance response of the equivalent circuit, the R_{sm} value was determined from the zero-phase angle region of the Bode plot. The remaining parameter values were chosen such that the discrepancy between simulated values of impedance (of the equivalent circuit model) and the measured value (of the cell) is minimized. In order to fit the equivalent circuit model into the experimental data, Simplex method for the Gamry echem analyst™ was used. Simplex method minimizes the χ^2 values to fit the impedance data to the modeled data using equivalent circuit model [35].

3.2.4 *Effect of temperature*

At all the other temperatures used in this work, the imaginary component of impedance showed frequency response similar to the one described above (Sect. 3.2.2) for 308 K. Thus, identical equivalent circuit was used to model the impedance response of the cell at these temperatures and the values of circuit elements were obtained using least square minimization. A comparison of the experimental and simulated values of impedances is shown in the form of Nyquist plot in Fig. 6a. A better idea of the curve fitting for a given model is obtained from the point based residual error ($\Delta Z/Z$) evaluation at each frequency. The residual errors ($\Delta Z/Z$) evaluated using the equivalent circuit evaluated values were found to be close to zero for both the real (Z_{real}) as well as the imaginary component (Z_{imag}). Residual error plot has been shown in Fig. 6b for the imaginary as well as real components of the impedance response at 308 K with the equivalent circuit model. It can be observed that the residual error for real and imaginary components are well within 0.0025–1 Hz. Scattering of the residual errors increases slightly beyond 1 Hz but is well within 0.01. Also the overall goodness of fit using the Gamry echem analyst™ software was found to be within the range of order 10^{-6}. Similar residual impedance response and the goodness of fit range was obtained for other temperature ranges. It may be seen from the figure that there exist a good agreement between the experimental and simulated values was obtained for all the temperatures. The values of power factor '*n*' for the CPE representing capacitive component was found to be close to 1, and for the CPE representing Warburg, it was found close to 0.5.

Figure 9 shows the different transport resistances at all the temperatures used for impedance measurement. Values of the ohmic resistances corresponding to solution and membrane resistance (R_{SM}), and leak resistances of DBL (R_{DBL}) and HT layer (R_{HT}) decreased with increase in the temperature of the cell. The maximum reduction was observed in R_{sm} value. The decrease in R_{HT} was much lower than that of the R_{DBL}. However, one important observation to be made is that the HT layer resistance values are comparable with the DBL resistance. This shows the resistance for the H^+ transport across the double layer of the membrane forms a significant fraction of the total resistance. The effect on the R_{SM} and R_{DBL} can be easily explained based on the increase in the thermal energy of the electroactive species along with an increase in ion mobility (increase in diffusion coefficient) with temperature. Similar trend has been reported in the literature for the EED cell for HI_x concentration, where the resistance of the EED cell was found to reduce along with temperature [16–19]. Impedance studies on the NaCl system by Długołecki et al. [25] reported similar findings of decrease in resistance components, which are consistent with our findings where temperature was found to affect the DBL and the ohmic resistance. The total resistance in a direct current operation is the sum of all the ohmic resistance components described in the equivalent circuit. As the electrical energy consumed in the EED cell is a function of the total potential drop across the EED cell, identification of the individual components is crucial toward the optimization of the EED process. From Fig. 9, it can be observed that the solution resistance dominates the overall resistance of the cell and also most affected with the increase in temperature. This provides an important deduction that in order to further reduce the DBL- and the HT-induced resistance, a different approach is needed for further reduction of the energy demands of the EED cell.

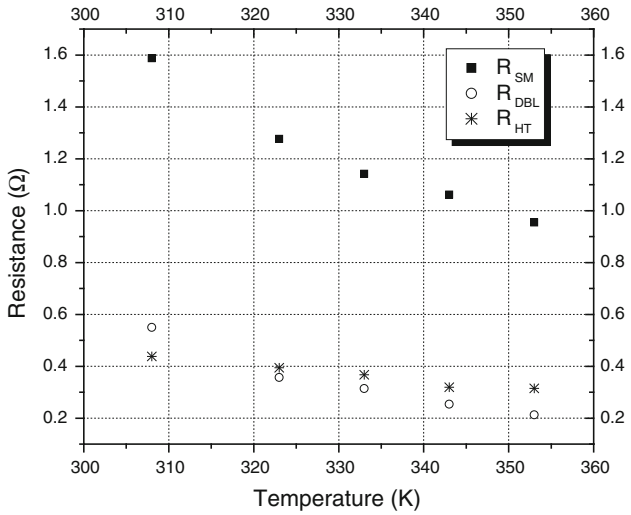

Fig. 9 Variation of the ohmic resistance components of the equivalent circuit with variation of the cell temperature from 308–353 K

Admittance values of the DBL and the HT layer at different temperatures are shown in Fig. 10. Admittance of the DBL remained nearly constant with the temperature. The HT admittance reduced with the increase in temperature. The heterogeneous transport layer was mainly due to EDL at membrane, and thus, it may be deduced that the reduction of admittance of HT was due to changes in EDL at the membrane. In order to evaluate the equivalent capacitance (C_{eq}) of circuit part, representing HT layer was evaluated for the parallel R_{HT}–CPE_{HT} element and was calculated as

$$C_{eq} = \frac{(Y_0 \times R)^{1/n}}{R} \tag{7}$$

The equivalent capacitance value reduced with temperature and the variation is shown in Fig. 11. This decrease could be an indication of decrease in the Donnan potential at higher temperature. A decrease in Donnan potential leads to decrease in selectivity of the membrane. This reduced selectivity can be the possible explanation for the observed reduction in current efficiency of EED cell as well as decrease in transport number for H^+ ions at higher temperature which has been reported in the literature [16, 19, 20].

Response of DBL and HT layer (in terms of voltage drop) has finite dynamics and takes time to develop fully on application of a DC current. A quantitative measure of the response time is the time constant (τ) of the corresponding parallel R–CPE circuit element. Using the relation between impedance ($Z = \frac{R}{1+(j\times\omega)^n \times R \times Y_0}$) and time constant ($Z = \frac{R}{1+(j\times\omega\times\tau)^n}$), the time constant of R–CPE element can be written as

$$\tau = (R \times Y_0)^{1/n} \tag{8}$$

Time constants for DBL and HT layer were calculated using Eq. 8 and their values at different temperature are shown in Fig. 12. The time constant values are indicative of the effective values of the resistance as well as the capacitive component associated with the process. Time constant in a parallel RC circuit are indicative of the time required to charge the capacitor to 63.2 %. The HT layer time constant was more than the DBL time constant, indicative of slower dynamics of the HT layer in comparison to the formation of the DBL. Also, both the time constants decreased with increase in temperature. The decrease in the time constant with temperature indicates that the dynamics increases with the increase in temperature owing to an increase in thermal energy of the electroactive species participating in the transport process.

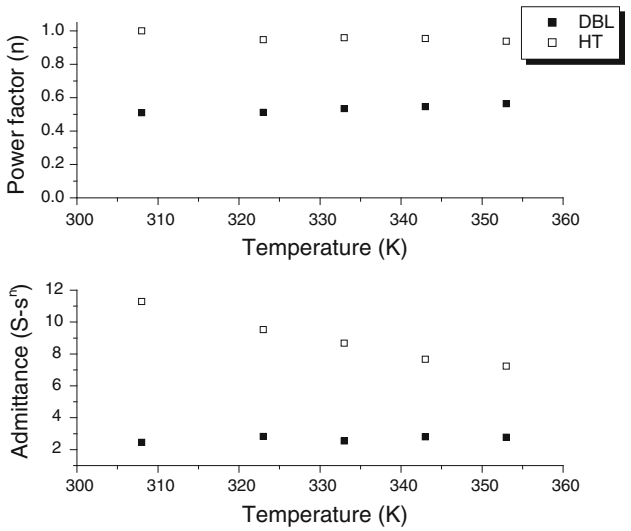

Fig. 10 Variation of the power factor (n) and admittance (Y_0) for DBL and the HT with variation of operating temperature from 308–353 K

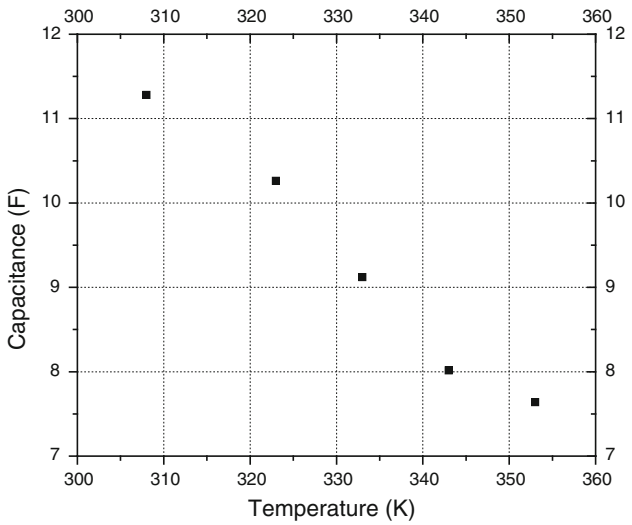

Fig. 11 Variation of the equivalent capacitance of the HT layer with cell temperature

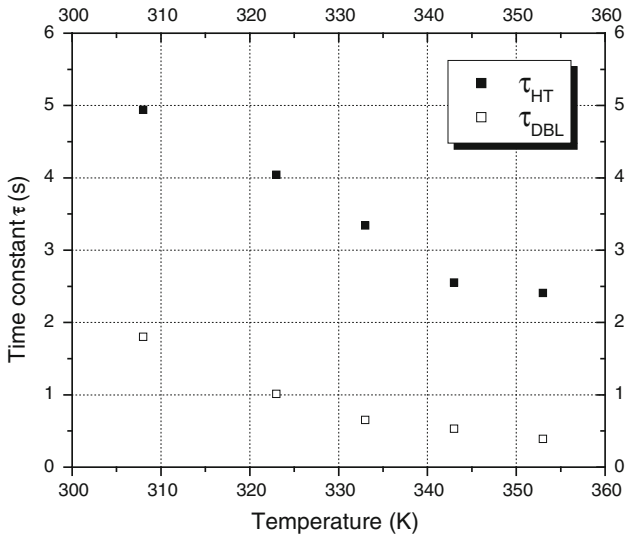

Fig. 12 Variation of the time constant for the HT layer and the DBL with temperature. The *filled symbols* represent the HT layer whereas the *unfilled symbols* represent the DBL

In the EED cell, reduction in DBL time constant is indicative of faster formation of DBL with increase in temperature.

4 Conclusion

Electrical impedance spectroscopic studies were conducted on single platinum electrode with varying area. Impedance of platinum electrode of different areas showed negligible contribution of the charge transfer resistance (R_{CT}) toward the total impedance response of the EED cell. Impedance response of a two-compartment EED cell used for concentration of HI_x solution was measured at four different temperatures. The obtained impedance response was modeled using an equivalent circuit after validating the linearity, causality, and stability using Kramers–Kronig transform. The equivalent circuit consisted of three parts, one for the ohmic resistance of the electrolyte and the membrane, the second for the DBL and third for the HT layer (non-electroneutral layer at the membrane). Ohmic resistance corresponding to DBL and solution and membrane as well as the HT was found to decrease with increase in the temperature of the cell. The admittance value for DBL was found to be fairly constant whereas for the HT layer it decreased with increase in temperature. Equivalent capacitance of the HT layer decreased with increase in temperature and could be an indicator of decreased Donnan potential and selectivity of membrane at higher temperature. Time constant for DBL was lower than HT layer and indicated faster dynamics of DBL compared to HT layer. Time constants for the two types of transport resistance decreased with increase in temperature.

Acknowledgments Authors (PKS, ANB, and AS) acknowledge the financial support from ONGC Energy Centre for carrying out this work.

References

1. Züttel A, Borgschulte A, Schlapbach L (2008) Hydrogen as a future energy carrier. Wiley, Weinheim
2. Jones LW (1970) Towards a liquid hydrogen fuel economy, University of Michigan engineering technical report UMR2320
3. Moriarty L, Honnery D (2007) Intermittent renewable energy: the only future source of hydrogen? Int J Hydrogen Energ 32: 1616–1624
4. Hirsch D, Steinfeld A (2004) Radiative transfer in a solar chemical reactor for the co-production of hydrogen and carbon by thermal decomposition of methane. Chem Eng Sci 59:5771–5778
5. Sverdrup JTG, Mann MK, Maness P-C, Kroposki B, Ghirardi M, Evans RJ, Blake D (2008) Renewable hydrogen production. Int J Energy Res 32:379–407
6. Dincer I, Tolga Balta M (2011) Potential thermochemical and hybrid cycles for nuclear-based hydrogen production. Int J Energy Res 35:123–137
7. Lewis MA, Masina JG, O'Hare PA (2009) Evaluation of alternative thermochemical cycles, Part I: the methodology. Int J Hydrogen Energ 34:4115–4124
8. Brown LC, Besenbruch GE, Lentsch RD, Schultz KR, Funk JF, Pickard PS, Marshall AC, Showalter SK (2003) High efficiency generation of hydrogen fuels using nuclear power. GA–A24285 (2003)
9. Norman JH, Besenbruch GE, O'Keefe DR (1981) Thermochemical water-splitting cycle for hydrogen production. GA-A 16713 (1981)
10. Giaconia A, Caputo G, Ceroli A, Diamanti M, Barbarossa V, Tarquini P, Sau S (2007) Experimental study of two phase separation in the Bunsen section of the sulfur–iodine thermochemical cycle. Int J Hydrogen Energ 32:531–536
11. Kasahara S, Kubo S, Onuki K, Nombra M (2004) Thermal efficiency evaluation of HI synthesis/concentration procedures in the thermochemical water splitting IS process. Int J Hydrogen Energ 29:579–587
12. Nomura M, Okuda H, Kasahara S, Nakao S-I (2005) Optimization of the process parameters of an electrochemical cell in the IS process. Chem Eng Sci 60:7160–7167
13. Hong S-D, Kim J-K, Bae K-K, Lee S-H, Choi H-S, Hwang G-J (2007) Evaluation of the membrane properties with changing iodine molar ratio in HI_x ($HI–I_2–H_2O$ mixture) solution to concentrate HI by electro-electrodialysis. J Membr Sci 291:106–110
14. Guo H, Kasahara S, Onuki K, Zhang P, Xu J (2011) Simulation study on the distillation of hyper-pseud azeotropic HI–I2–H2O mixture. Ind Eng Chem Res 50:11644–11656
15. Onuki K, Hwang G-J, Shimizu S (2000) Electrodialysis of hydriodic acid in the presence of iodine. J Membr Sci 175: 171–179
16. Onuki K, Hwang G-J, Shimizu Arifal S (2001) Electro-electrodialysis of hydriodic acid in the presence of iodine at elevated temperature. J Membr Sci 192:193–199
17. Yoshida M, Tanaka N, Okuda H, Onuki K (2008) Concentration of HIx solution by electro-electrodialysis using Nafion 117 for thermochemical water-splitting IS process. Int J Hydrogen Energ 33:6913–6920
18. Sow PK, Shukla A (2012) Effect of asymmetric variation of operating parameters on EED cell for HI concentration in I-S cycle for hydrogen production. Int J Hydrogen Energ 37: 13958–13970

19. Sow PK, Shukla A (2012) Electro-electrodialysis for concentration of hydriodic acid. Int J Hydrogen Energ 37:3931–3937
20. Hong S-D, Kim C-H, Kim J-G, Lee S-H, Bae K-K, Hwang G-J (2006) HI concentration from HIx (HI–H2O–I2) solution for the thermochemical water-splitting IS process by electro- electrodialysis. J Ind Eng Chem 12:566–570
21. Park JS, Choi JH, Woo JJ, Moon SH (2006) An electrical impedance spectroscopic (EIS) study on transport characteristics of ion-exchange membrane systems. J Colloid Interface Sci 300: 655–662
22. Park J-S, Choi JH, Yeon KH, Moon SH (2006) An approach to fouling characterization of an ion-exchange membrane using current–voltage relation and electrical impedance spectroscopy. J Colloid Interface Sci 294:129–138
23. Gomadam PM, Weidner JW (2005) Analysis of electrochemical impedance spectroscopy in proton exchange membrane fuel cells. Int J Energy Res 29:1133–1151
24. Chilcott TC, Chan M, Gaedt L, Nantawisarakul T, Fane AG, Coster HGL (2002) Electrical impedance spectroscopy characterization of conducting membranes: I Theory. J Membr Sci 195: 153–167
25. Długołecki P, Ogonowski P, Metz SJ, Saakes M, Nijmeijer K, Wessling M (2010) On the resistances of membrane, diffusion boundary layer and double layer in ion exchange membrane transport. J Membr Sci 349:369–379
26. Sow PK, Sant S, Shukla A (2010) EIS studies on electro-electrodialysis cell for concentration of hydriodic acid. Int J Hydrogen Energ 35:8868–8887
27. Moya AA (2012) Electric circuits modeling the low-frequency impedance of ideal ion-exchange membrane systems. Electrochim Acta 62:296–304
28. Moya AA (2011) Influence of dc electric current on the electrochemical impedance of ion-exchange membrane systems. Electrochim Acta 56:3015–3022
29. Moya AA (2010) Study of the electrochemical impedance and the linearity of the current–voltage relationship in inhomogeneous ion-exchange membranes. Electrochim Acta 55:2087–2092
30. Nikonenko VV, Kozmai AE (2011) Electrical equivalent circuit of an ion-exchange membrane system. Electrochim Acta 56: 1262–1269
31. Sistat P, Kozmaib A, Pismenskayab N, Larchet C, Pourcellya G, Nikonenkob V (2008) Low-frequency impedance of an ion-exchange membrane system. Electrochim Acta 53:6380–6390
32. Bard AJ, Faulkner LR (2004) Electrochemical methods: fundamentals and applications, 2nd edn. Wiley, Weinheim
33. Orazem ME, Tribollet B (2008) Electrochemical impedance spectroscopy, 1st edn. Wiley, New Jersey
34. Boukamp BA (1995) A linear Kronig–Kramers transform test for immittance data validation. J Electrochem Soc 142:1885
35. http://www.gamry.com/
36. Sang S, Wu Q, Huang K (2008) A discussion on ion conductivity at cation exchange membrane/solution interface. Colloids Surfaces A: Physiochem Eng Aspects 315:98–102